Available online at www.sciencedirect.com

ScienceDirect

Procedia IUTAM 12 (2015) 145 – 153

Procedia IUTAM

www.elsevier.com/locate/procedia

IUTAM Symposium on Mechanics of Soft Active Materials

Mechanics of bio–hybrid systems

P. Nardinocchi[a,*], M. Pezzulla[a], L. Teresi[b]

[a]*Dipartimento di Ingegneria Strutturale e Geotecnica, Sapienza Università di Roma, via Eudossiana 18, I-00184 Roma, Italy*

[b]*LaMS - Modeling & Simulation Lab, Dipartimento di Matematica e Fisica, Università degli Studi Roma Tre, via della Vasca Navale 84, I-00146 Roma, Italy*

Abstract

Bio–hybrid system are morphing structures whose shaping can be electrically driven and strongly depends on the geometrical and mechanical characteristics of the system. The estimation of those characteristics which allow for getting target shapes is a great challenge. We present and discuss an approximate model for narrow bio–hybrid strips which works well in plane bending. A generalization towards three–layers bio–hybrid system is presented.

Peer-review under responsibility of Konstantin Volokh and Mahmood Jabareen.

Keywords: active soft materials, bio–hybrid systems, inverse shaping problem.

1. Introduction

Bio–hybrid systems are generated from the assembly of biological active materials and synthetic polymers, and can be used both as soft actuators and to investigate a biological system, through the analysis of its structure, function, and working conditions.[1,2] In particular, we have in mind bio–hybrid systems based on the muscular thin film (MTF) technique, which enables cardiac myocytes to be engineered on a thin flexible substrate.[3] From the point of view of continuum mechanics, those bio-hybrid systems may be viewed as soft morphing three-dimensional systems whose shaping can be electrically driven, and depends on the geometrical and mechanical characteristics of the system as well as on the orientation of the cardiac myocites. A key issue concerns the estimation of the characteristics of the system which enable to get, under electrical stimulus, three–dimensional shapes.[4,5]

In the past, we proposed an electromechanical modeling of those bio–hybrid systems, set within the context of finite elasticity with large distortions, based on the following points: (1) muscle tissue contractions are described through distortions; (2) distortions are driven by the propagation of the action potential (AP) within MTF through an excitation-contraction coupling model; (3) the propagation of the AP is ruled by an ionic model consisting of a system of two reaction-diffusion equations (RDEs).[6,5] Therein, we also set the inverse shaping problem for a specific bio–hybrid system;[1] our aims were to calculate the distortion field necessary to produce a target shape, for a given

* Corresponding author. Tel.: +39-0644585242; fax: +39-064884852.
E-mail address: paola.nardinocchi@uniroma1.it

Peer-review under responsibility of Konstantin Volokh and Mahmood Jabareen.
doi:10.1016/j.piutam.2014.12.016

set of design parameters (both geometrical and mechanical), and determine an admissible range of design parameters corresponding to the same solution.

In the present paper, we propose an approximate model for bio–hybrid narrow strips which allows to describe bending performances of those systems, and to analytically set and solve the inverse shaping problem. The comparison of the outcomes of the model with the fully three–dimensional nonlinear model above cited is discussed. At the end, a proof–of–concept based on three–layers bio–hybrid strips capable to twist and generate helicoid–like and ribbon–like shapes is discussed.

2. Background

A bio–hybrid system consists of a passive and a biological active layer working in parallel. When an external electrical stimulus activates the myocytes in the biological layer, the cells contract; the global effect of the contraction may be either the stretching or the bending of the specimen. For the material and geometrical characteristics of the layers of MTF, the minimum energy state corresponds to the bending of the bilayer system; the magnitude of the bending is affected by the geometrical and mechanical properties of the system, whereas the flexure plane is determined by the direction of the myocytes. When the direction of the myocytes is fixed, the design of the bio–hybrid system involves the *design parameters* $(h_a, E_a; h_p, E_p)$ representing the thickness and the elastic modulus of the active and the passive layers, respectively. Among the questions to be investigated there is the determination of the admissible range of the design parameters yielding a target bent shape. Even if myocites contraction is driven by the electrical potential, it has well–known biological limits; hence, the design problem can be set considering only the elastic problem of the bio–hybrid system, with the myocytes contraction acting as a datum.

2.1. Mechanics

The mechanical behavior of both the active and passive layers of the bio–hybrid system can be set within the context of three–dimensional (3D), incompressible, nonlinear elasticity with large distortions.[7] To this aim, we introduced the time line $\mathcal{T}$ and the three–dimensional Euclidean ambient space $\mathcal{E}$ and identified the bilayer system with a three–dimensional body manifold $\mathcal{B} \subset \mathcal{E}$, whose motion is described by the position–valued field

$$p : \mathcal{B} \times \mathcal{T} \to \mathcal{E}, \quad (y, \tau) \mapsto x = p(y, \tau), \tag{2.1}$$

assigning to each material point $y \in \mathcal{B}$ and time $\tau \in \mathcal{T}$ a place $x \in \mathcal{E}$ that is referred to as the place occupied by y at time τ. Denoted with $\mathcal{V}$ the translation space of $\mathcal{E}$ and with $\mathbf{u} : \mathcal{B} \times \mathcal{T} \to \mathcal{V}$ the displacement field, it holds: $x = y + \mathbf{u}(y, \tau)$. We described distortions through the introduction of a smooth tensor–valued field $\mathbf{F}_o : \mathcal{B} \to \mathbb{L}\mathtt{in}$ with positive Jacobian determinant $J_o := \det \mathbf{F}_o > 0$. The distortion field $\mathbf{F}_o$ was assumed to be anisotropic, to account for the anisotropic structure of the biological layer; moreover, as contractions of the myocytes are isochoric, $\mathbf{F}_o$ was assumed volume–preserving, *i.e.* $J_o = 1$. Denoted with ε the shortening of the myocytes, we wrote:

$$\mathbf{F}_o(\varepsilon, y) = (1 - \varepsilon)\, \mathbf{a}(y) \otimes \mathbf{a}(y) + \frac{1}{\sqrt{1 - \varepsilon}} (\mathbf{I} - \mathbf{a}(y) \otimes \mathbf{a}(y)), \tag{2.2}$$

where $\mathbf{a}$ is a material unit vector field denoting the direction of the myocytes. Typically, the largest shortening that can be expected from cardiac cells is about 0.3 (30%); hence, the admissible range for ε is assumed to be $(0, 0.3)$. We defined the elastic deformation $\mathbf{F}_e$ as the difference, in the sense of the multiplicative decomposition, between the visible deformation $\mathbf{F}$ and the distortion $\mathbf{F}_o$: $\mathbf{F}_e = \mathbf{F}\, \mathbf{F}_o^{-1}$. The local and exact strain measure to be used in the theory of finite elasticity with distortions is

$$\mathbf{C}_e = \mathbf{F}_e^T\, \mathbf{F}_e = \mathbf{F}_o^T\, \mathbf{C}\, \mathbf{F}_o^{-1}, \tag{2.3}$$

with $\mathbf{C} = \mathbf{F}^T\, \mathbf{F}$ the standard strain measure of finite elasticity. We assumed that the free–energy density ψ_o per unit relaxed volume $dV_o = J_o\, dV$ is a function of the elastic deformation $\mathbf{F}_e$: $\psi_o(y, \tau) = \psi_o(\mathbf{F}_e(y, \tau))$. Given ψ_o, and granted for the multiplicative decomposition of the deformation gradient, the strain energy density per unit reference volume ψ may be represented as a function of $\mathbf{F} = \mathbf{F}_e\, \mathbf{F}_o$, defined by

$$\psi(y, \tau) = J_o(y)\, \psi_o(\mathbf{F}_e(y, \tau)). \tag{2.4}$$

We described the incompressible material response through the nearly incompressible material model based on the splitting of the strain energy density ψ_o into a purely isochoric ψ_{os} and a volumetric contribution ψ_{ov} such that[8]

$$\psi_o(\mathbf{F}_e) = \psi_{os}(\mathbf{F}_s) + \psi_{ov}(J_e)\,, \quad \mathbf{F}_s = J_e^{-1/3}\mathbf{F}_e\,, \quad J_e = \det \mathbf{F}_e\,. \tag{2.5}$$

Specifically, we assumed that

$$\psi_{os}(\mathbf{F}_s) = \frac{1}{2}\mu(\mathbf{F}_s \cdot \mathbf{F}_s - 3)\,, \quad \psi_{ov}(J_e) = \frac{1}{2}k(J_e - 1)^2\,; \tag{2.6}$$

μ is the shear modulus of the material, and k is the bulk modulus, assumed to be much larger than μ to approximate material incompressibility. The reference stress $\mathbf{S}$ took the following constitutive representation:

$$\mathbf{S} = \frac{\partial \psi}{\partial \mathbf{F}} = \mu J_e^{-2/3}\mathbf{F}_e\Big(\mathbf{I} - \frac{1}{3}(\mathbf{C}_e \cdot \mathbf{I})\mathbf{C}_e^{-1}\Big) - p\mathbf{F}^{\star}\,, \quad p = -k(J_e - 1)\,. \tag{2.7}$$

The direct problem of elasticity consisted in the following: given $\mathbf{F}_o$, find the displacement $\mathbf{u}$ that solves the balance equations $\mathrm{Div}\,\mathbf{S} = \mathbf{0}$ in $\mathcal{B}$, and satisfies appropriate boundary conditions on $\partial\mathcal{B}$. The inverse problem can be formulated as: given the displacement $\mathbf{u}$, find the design parameters which are needed to realize that $\mathbf{u}$ under a physiological range of contraction ε. The outcomes of the numerical implementation of the model are discussed together with the results of the approximate model below presented.

3. Bio–hybrid narrow strips under plane bending

As design problem in bio-hybrid systems may be expensive, when managed by FE simulations, we present and discuss a one–dimensional approximated model to described plane bending of bio–hybrid beam–like systems. Precisely, the plane bending is driven by two parameters which represent the active contraction of the myocites layer and a possible pre stretch within the passive elastomeric layer.

Figure 1 shows a sketch of the muscular thin film (MTF) whose plane bending we are going to study. The thickness of the MTF is denoted as h and it is equal to the sum of the thicknesses h_p and h_a of a top passive and a bottom active layer, respectively. Correspondingly, we denote as E_p and E_a the Young moduli of the two layers. The two key parameters at the center of our design problem are the thicknesses and Young moduli ratios: $m = h_a/h_p$ and $\alpha = E_a/E_p$. Assuming fixed the thickness h_a and the Young modulus E_a of the myocites layer, the parameters m and α are directly related to the thickness h_p and the Young modulus E_p of the passive layer. We assume that the plane

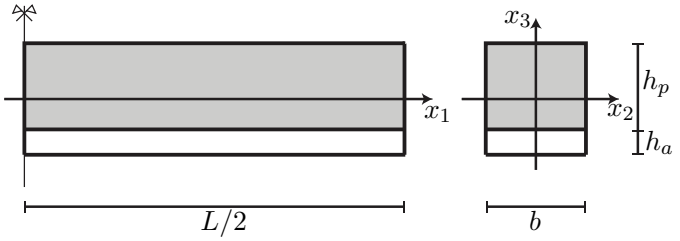

Figure 1. Sketch of a bio–hybrid narrow strip: h_a and h_p measure the thicknesses of the active and passive layer, respectively.

$x_2 = 0$ is the flexure plane and that beam's cross sections stay flat. With this, the longitudinal stretch $\lambda(x_1, x_3)$ suffered by the longitudinal fibers may be represented as

$$\lambda(x_1, x_3) = \Lambda_o(x_1) + x_3\Lambda_1(x_1)\,, \quad \Lambda_1 = \Lambda_0^2\kappa\,, \tag{3.8}$$

with Λ_0 and κ the possibly large longitudinal stretch and curvature of the beam axis ($\kappa > 0$).[1] It is assumed that the longitudinal visible stretch can be multiplicatively split into an elastic and an inelastic factor: $\lambda = \lambda_e\lambda_o$; the

[1] It is worth noting that it should be $\lambda = \Lambda_o(1 + y_3\kappa)$, being y_3 the coordinate along the beam thickness corresponding to x_3 in the deformation process; we assumed that $y_3 = \Lambda_o\, x_3$.

decomposition holds within each layer of the system, also if the inelastic component λ_o may well assume a different physical meaning within the two layers. In particular, we consider the distortion of the passive layer as representing a pre–stretch, possibly prior to the activation–induced bending, whereas the distortion of the active layer is assumed to model the active shortening of the myocytes, when electrically stimulated. From now on, we denote the distortion inside the passive layer as $\lambda_o^{\rm ps}$ and assume it always larger than 0 ($\lambda_o^{\rm ps} > 0$). Moreover, we denote the distortion of the cardiac tissue as $1-\varepsilon$, being ε the shortening of the muscle cells, taking the value 0 when the muscle cells stay in their rest state.

So, only looking at the longitudinal deformations mismatch due to $\lambda_o^{\rm ps}$ and ε and considering it as the main cause of the bending of the system, we assume that the total energy of the system can be represented as

$$\mathcal{E} = \frac{1}{2} b \int_{-\frac{h}{2}}^{\frac{h}{2}-\beta h} E_b\Big(\frac{\lambda}{1-\varepsilon} - 1\Big)(1-\varepsilon) dx_3 + \frac{1}{2} b \int_{\frac{h}{2}-\beta h}^{\frac{h}{2}} E_t\Big(\frac{\lambda}{\lambda_o^{\rm ps}} - 1\Big)\lambda_o^{\rm ps} dx_3 \,. \tag{3.9}$$

We look for uniform longitudinal stretch and beam curvature, plug equation (3.8) into (3.9), and represent the functional $\mathcal{E}$ as a function of the two variables Λ_o and Λ_1 as

$$\begin{aligned}\mathcal{E} = \frac{1}{2}\mathbb{B}_p f(m,\alpha,\varepsilon,\lambda_o^{\rm ps})\Lambda_1^2 + \frac{1}{2}\mathbb{A}_p m h_p\Big(\frac{\Lambda_o - \lambda_o^{\rm ps}}{\lambda_o^{\rm ps}} - \frac{\alpha}{1-\varepsilon}(\Lambda_o - (1-\varepsilon))\Big)\Lambda_1 + \\ \frac{1}{2}\mathbb{A}_p\Big(\frac{(\Lambda_o - \lambda_o^{\rm ps})^2}{\lambda_o^{\rm ps}} + \frac{\alpha m}{1-\varepsilon}(\Lambda_o - (1-\varepsilon))^2\Big),\end{aligned} \tag{3.10}$$

where

$$f(m,\alpha,\varepsilon,\lambda_o^{\rm ps}) = \frac{1}{\lambda_o^{\rm ps}} + 3\alpha m \frac{1}{1-\varepsilon} + 3m^2 \frac{1}{\lambda_o^{\rm ps}} + \alpha m^3 \frac{1}{1-\varepsilon}\,, \tag{3.11}$$

whereas $\mathbb{A}_p = b h_p E_p$ and $\mathbb{B}_p = 1/12 b h_p^3 E_p$ are the axial and bending stiffnesses of the passive top layer. The corresponding Euler–Lagrange equations deliver the following linear system in the unknown Λ_o and Λ_1:

$$\begin{aligned}\mathbb{A}_p\Big(\frac{1}{\lambda_o^{\rm ps}} + m\frac{\alpha}{1-\varepsilon}\Big)\Lambda_o + \frac{1}{2}\mathbb{A}_p m h_p\Big(\frac{1}{\lambda_o^{\rm ps}} - \frac{\alpha}{1-\varepsilon}\Big)\Lambda_1 = \mathbb{A}_p(1+\alpha m)\,, \\ \frac{1}{2}\mathbb{A}_p m h_p\Big(\frac{1}{\lambda_o^{\rm ps}} - \frac{\alpha}{1-\varepsilon}\Big)\Lambda_o + \mathbb{B}_p f(m,\alpha,\varepsilon,\lambda_o^{\rm ps})\Lambda_1 = \frac{1}{2}\mathbb{A}_p m h_p(1-\alpha)\,.\end{aligned} \tag{3.12}$$

Remark. Let us note that the longitudinal stresses corresponding to the energy functional (3.9), are

$$\begin{aligned}\sigma_a(x_1,x_3) = E_a\Big(\frac{\lambda(x_1,x_3)}{1-\epsilon} - 1\Big), \quad -\frac{h}{2} < x_3 < \Big(\frac{h}{2} - \beta h\Big), \\ \sigma_p(x_1,x_3) = E_p\Big(\frac{\lambda(x_1,x_3)}{\lambda_o^{\rm ps}} - 1\Big), \quad \Big(\frac{h}{2} - \beta h\Big) < x_3 < \frac{h}{2}\,,\end{aligned} \tag{3.13}$$

in the active and passive layer, respectively. Moreover, under no external loads, the total force and total moment on each cross section of the beam must be equal to zero:

$$\begin{aligned} b\int_{-\frac{h}{2}}^{\frac{h}{2}-\beta h} \sigma_a(x_1,x_3)dx_3 + b\int_{\frac{h}{2}-\beta h}^{\frac{h}{2}} \sigma_p(x_1,x_3)dx_3 = 0 \\ b\int_{-\frac{h}{2}}^{\frac{h}{2}-\beta h} x_3\sigma_a(x_1,x_3)dx_3 + b\int_{\frac{h}{2}-\beta h}^{\frac{h}{2}} x_3\sigma_p(x_1,x_3)dx_3 = 0\,.\end{aligned} \tag{3.14}$$

Equations (3.14) deliver the same linear system shown in 3.12. •

The solution of the linear system (3.12) may be expressed in the following form

$$\Lambda_o = \check{\Lambda}_o(\varepsilon,\lambda_o^{ps};m,\alpha) \quad \text{and} \quad \Lambda_1 = \check{\Lambda}_1(\varepsilon,\lambda_o^{ps};m,\alpha,h_a)\,, \tag{3.15}$$

with

$$\check{\Lambda}_o(\varepsilon,\lambda_o^{ps};m,\alpha)=\frac{(\varepsilon-1)\lambda_o^{\rm ps}(\varepsilon(1+\alpha m a(m))-1)-\alpha m(a(m)+\lambda_o^{\rm ps}(3+m(3+m+\alpha m^2)))}{1+\varepsilon^2-2\varepsilon(1+\alpha\lambda_o^{\rm ps}mc(m))+\alpha\lambda_o^{\rm ps}m(4+m(6+m(4+\alpha\lambda_o^{\rm ps}m)))},$$

$$\check{\Lambda}_1(\varepsilon,\lambda_o^{ps};m,\alpha,h_a)=\frac{6}{h_t}\frac{\alpha m(1-\varepsilon)\lambda_o^{\rm ps}(\varepsilon-1+\lambda_o^{\rm ps})(1+m)}{1+\varepsilon^2-2\varepsilon(1+\alpha\lambda_o^{\rm ps}c(m))+\alpha\lambda_o^{\rm ps}m(4+m(6+m(4+\alpha\lambda_o^{\rm ps}m)))}, \tag{3.16}$$

where $a(m)=1+3m(1+m)$ and $c(m)=2+m(3+2m)$. We compare this solution with the one derived via finite element implementation of the corresponding fully 3D nonlinear model already presented.[5] We choose the beam sample as 1 mm long, 1 μm wide and 26 μm thick, a longitudinal alignment of the myocites, and an the aspect ratio $h/b>1$ (it is a critical parameter that defines the range of applicability of the 1D model). Figure 3 shows the comparison between the analytical and the numerical solutions in terms of the longitudinal axis stretch Λ_o and the curvature $\kappa=\Lambda_1/\Lambda_o^2$, corresponding to $m=2/9$ and $\alpha=0.04$. The solution is plotted versus the shortening ε for two different values of the pre–stretch $\lambda_o^{\rm ps}$ $(=1,1.1)$. It is worth noting that, for $\varepsilon=0$, the longitudinal axis stretch is approximately equal to $\lambda_o^{\rm ps}$ whereas the curvature κ is zero if and only if $\lambda_o^{\rm ps}=1$. Beam's curvature is also plotted versus m and α, for different

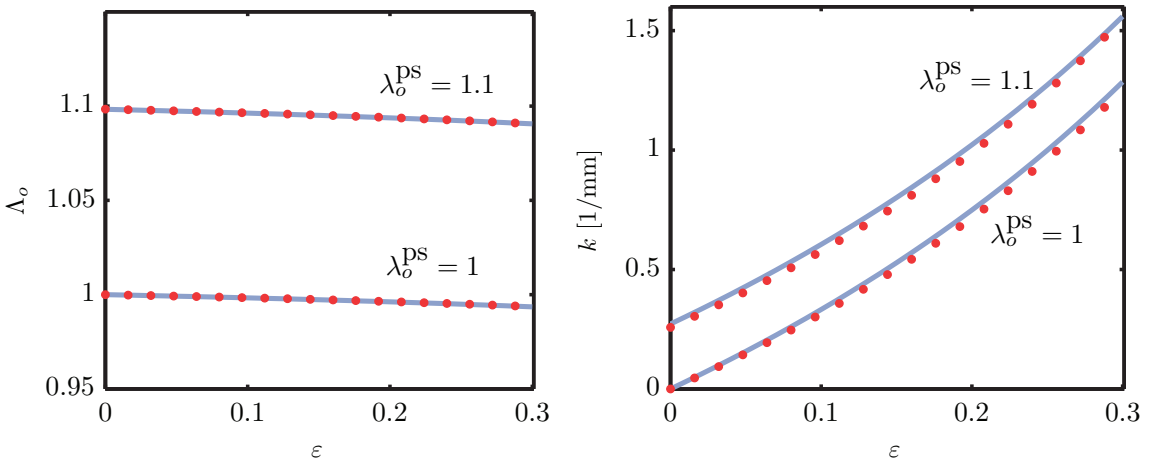

Figure 2. Comparison between analytical (solid lines) and numerical solutions (dots): longitudinal axis stretch Λ_o (left) and curvature κ (right).

values of α and m, respectively, with all the other parameters fixed. The curvature increases monotonically with both m and α.

Our simple 1D model may also be used to compute the time course of the beam's curvature κ when the time courses of the pre–stretch λ_o^{ps} and the shortening ε are assigned. For example, if $\varepsilon(t)=0.3\sin^2(\pi f t)$ and $\lambda_o^{\rm ps}=1+0.1(1-\exp(-t/\tau))$, the curvature of the system is depicted in figure 4 (left) when $f=1$ Hz and $\tau=0.2$ s [1,2]. Finally, a comparison between our 1D model and the results of the theory of bimetallic thermostats[9] is presented. This theory prescribes that the curvature depends on α and m as

$$\kappa\sim\frac{6}{h}\frac{1}{3+(1+m\alpha^{-1}/(1-m))(m^2+\alpha(1-m)^3/m)}. \tag{3.17}$$

This relationship between κ and the couple (α,m) does not involve the shortening and the pre–stretch; therefore, for a fixed value of the couple $(\varepsilon,\lambda_o^{\rm ps})$, a scaling factor should be chosen to make a comparison between our 1D model and the theory of bimetallic thermostats.

Figure 4 (right) shows the comparison between the Timoshenko model and our 1D model for $\lambda_o^{\rm ps}=1$ and $\varepsilon=(0.15,0.3)$: the agreement is very good and the scaling factor depends almost linearly on ε.

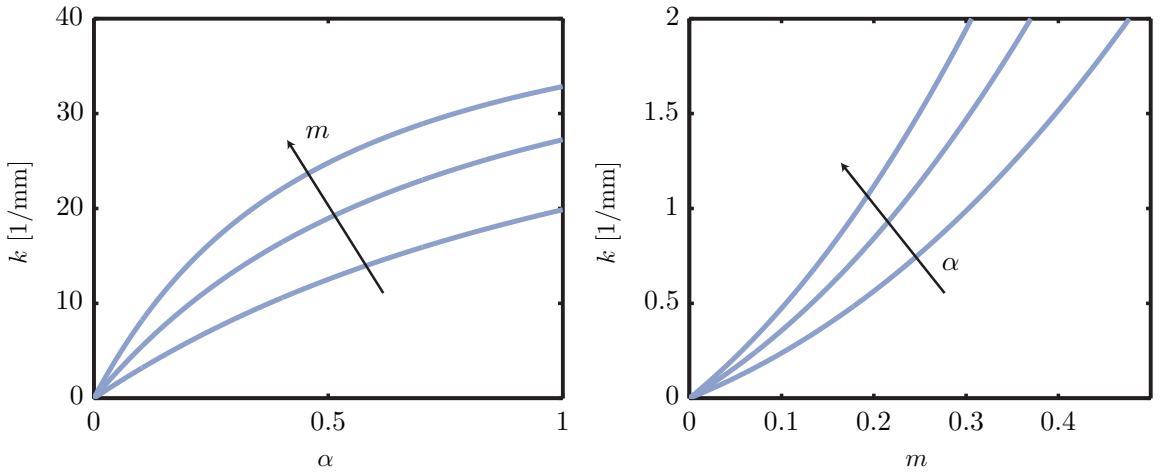

Figure 3. Curvature κ versus α for different values of $m = 2/9, 3/9, 4/9$ at $\varepsilon = 0.3$ (left); curvature κ versus m for different values of $\alpha = 0.02, 0.03, 0.04$ at $\varepsilon = 0.3$ (right).

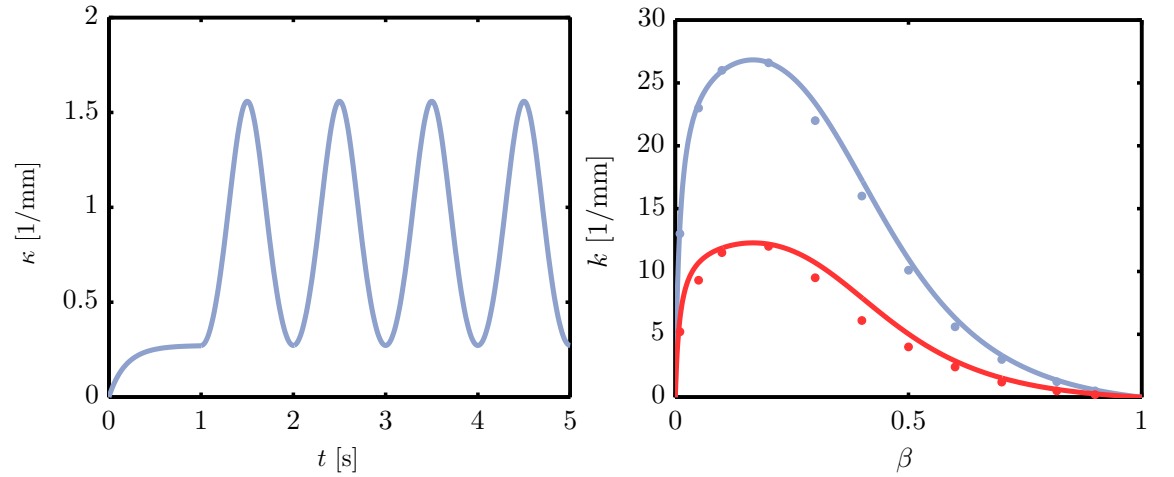

Figure 4. Time course of the curvature κ for a 1 Hz shortening signal and an exponential law for the pre–stretch (left). Comparison between the theory of bimetallic thermostats (curves) and our 1D model (dots) for $\lambda_o^{\rm ps} = 1$ and $\varepsilon = 0.15$ (red) and $\varepsilon = 0.3$ (blue) (right).

3.1. Shape control

As discussed in the Introduction, the design of a bio–hybrid system is a crucial task to determine the admissible range of the design parameters in order to achieve the target shape of the specimen. In terms of our 1D model, we look for a range of the design parameters that correspond to a particular solution of the problem $(\Lambda_o^\star, \Lambda_1^\star)$, attained for $\varepsilon = \varepsilon^\star$, $\alpha = \alpha^\star$, $m = m^\star$, and $h_a = h_a^\star$. Approximating the longitudinal stretch of the beam by the pre–stretch, the problem can be stated as follows:[2] find the relation between α and m such that, for a fixed value of the pre–stretch $\lambda_o^{\rm ps}$, the following relation holds

$$\kappa(\lambda_o^{\rm ps}, \alpha, m, h_a) = \kappa^\star\,, \tag{3.18}$$

[2] In particular, for small m, the longitudinal stretch may be expressed as $\Lambda_o = \lambda_o^{\rm ps} + \alpha\lambda_o^{\rm ps}\left(1 + \frac{\lambda_o^{\rm ps}}{\varepsilon - 1}\right)m + O(m^2)$ and it is always smaller than the pre–stretch $\lambda_o^{\rm ps}$.

with $\kappa^\star$ the curvature corresponding to $(\Lambda_o^\star, \Lambda_1^\star)$. Figure 5 shows the solution of this problem for different values of $\kappa^\star = 1, 1.285, 1.4$ mm^{-1} and $\lambda_o^{\rm ps} = 1$. In particular, we show both the solution of the complete problem (red dotted lines), given by the appropriate inversion of the equations (3.16) and the solution corresponding to the approximation $\Lambda_o \simeq \lambda_o^{ps}$ (blue solid lines). In this latter case, curves may be explicitly written as

$$\begin{aligned}\alpha = -\frac{1}{h_t\kappa^\star\lambda_o^{ps\,3}m^4}\Big(\big((\varepsilon-1)^2m^2(1+m)(-3(1+m)+3\varepsilon(1+m)+3\lambda_o^{\rm ps}(1+m)\\ -2h_t\kappa^\star\lambda_o^{\rm ps\,2}(1+m+m^2))(-3+3\varepsilon+\lambda_o^{\rm ps}(3-2h_t\kappa^\star\lambda_o^{\rm ps}(1+m)))\big)^{1/2}\\ +(\varepsilon-1)m\Big(3(1+m)-3\varepsilon(1+m)-3\lambda_o^{\rm ps}(1+m)+h_t\kappa^\star\lambda_o^{\rm ps\,2}(2+m(3+2m))\Big)\Big).\end{aligned} \tag{3.19}$$

Within the range considered for the parameter m, the exact and approximate solutions are practically coincident. Each curve divides the $m-\alpha$ plane into 2 parts: the top part consists of the pairs (α, m) which determine a curvature $\kappa > \kappa^\star$, whereas the bottom part consists of the pair (α, m) which determine a curvature $\kappa < \kappa^\star$.

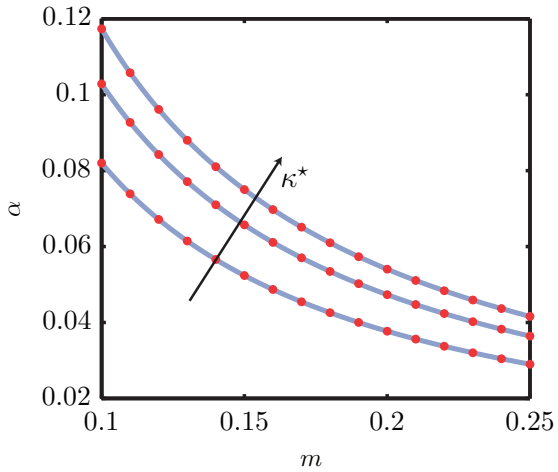

Figure 5. Approximate (blue solid lines) and exact (red dotted line) iso–solution curves in the plane (α,m) corresponding to $\kappa^\star = 1, 1.285, 1.4$ mm^{-1}.

4. Three–layers bio–hybrid narrow strips

We propose, as a proof–of–concept, a new architecture for a bio–hybrid system consisting of a passive and two biological active layers working in parallel, with the passive as the middle layer. We assume that the direction of the myocites is fixed in such a way that on the top layer myocites are oriented roughly at 45° to the strip axis and on the bottom layer are oriented perpendicularly to the top myocites (see figure 6). We expect that when an external

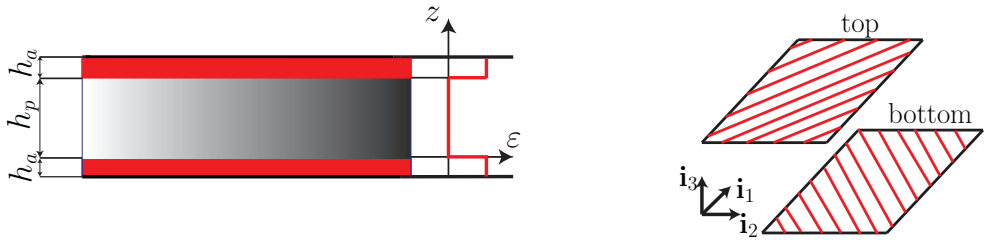

Figure 6. Sketch of a three–layers bio–hybrid narrow strip: h_a and h_p measure the thicknesses of the active and passive layer, respectively..

electrical stimulus activates the myocytes in the biological layers, the global effect of the contraction is a deformation

more complex than the plane bending shown in the previous section. Actually, driven by results got for different soft systems with the same key stiffer microstructure, we expect to get helicoid–like shapes and ribbon–like shapes, depending on the aspect ratio of the strip. [10,11,12]

Before solving the electro–mechanical problem, with the myocites's shortening driven by an electric stimulus, we deal with the elastic problem of the system with the aim to understand which mechanical and geometrical parameters, apart from the aspect ratio, drive the final shape of the strip. We implemented the three–dimensional fully nonlinear elastic problem already presented and shortly summed up in the Background section. [5] The problem was solved via a commercial finite element code using quartic elements for the displacement vector and linear elements for the pressure field. The mesh consists of 1200 elements corresponding to 35000 degrees of freedom.

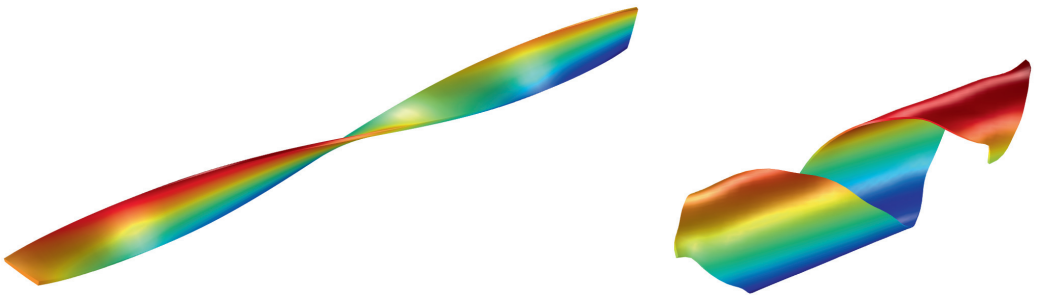

Figure 7. Helicoid–like (left) and ribbon–like (right) shapes correspond to two different aspect ratio $b/h = 15, 77$, respectively.

We assigned a one–parameter family of increasing shortening ε, going from 0 to 0.3, and solved the corresponding one–parameter family of elastic problems starting from a flat reference configuration. Figure 7 shows the final shapes got from two strips with different aspect ratios: on the left the helicoid–like shape corresponding to the smaller aspect ratio ($b/h = 15$) and on the right the ribbon–like shape corresponding to the larger aspect ratio ($b/h = 77$).

Understanding the dependence of the other key geometrical factors such as the number of pitches in the ribbon–like shape and the number of nodes in the helicoid–like shape is crucial to get shape control. However, each numerical simulation is extremely heavy and, in our opinion, the shape control task can't be got through finite element implementations. Explicit analyses based on the study of the energy functional corresponding to the two systems can be done, following what already done for other systems. [10,11] Of course, in this case, approximated solutions have to be chosen, which can qualitatively and quantitatively describe the three–dimensional behavior of the systems, as shown in the case of the two–layers bio–hybrid system under plane bending.

Acknowledgements

The work is supported by Sapienza Università di Roma through the grant N. C26A11STT5.

References

1. Nawroth, J.C., Lee, H., Feinberg, A.W., Ripplinger, C.M., McCain, M.L., Grosberg, A., et al. A tissue-engineered jellyfish with biomimetic propulsion. *Nat Biotech* 2012;**30**(8):792–797. URL: http://dx.doi.org/10.1038/nbt.2269.
2. Shim, J., Grosberg, A., Nawroth, J.C., Kit Parker, K., Bertoldi, K.. Modeling of cardiac muscle thin films: Pre-stretch, passive and active behavior. *Journal of Biomechanics* 2012;**45**(5):832–841. URL: http://www.sciencedirect.com/science/article/pii/S0021929011007068.
3. Feinberg, A.W., Feigel, A., Shevkoplyas, S.S., Sheehy, S., Whitesides, G.M., Parker, K.K.. Muscular thin films for building actuators and powering devices. *Science* 2007;**317**(5843):1366–1370. URL: http://www.sciencemag.org/content/317/5843/1366.full.pdf. doi:10.1126/science.1146885.
4. Alford, P.W., Feinberg, A.W., Sheehy, S.P., Parker, K.K.. Biohybrid thin films for measuring contractility in engineered cardiovascular muscle. *Biomaterials* 2010;**31**(13):3613–3621. URL: http://www.sciencedirect.com/science/article/pii/S0142961210001110.
5. Lucantonio, A., Nardinocchi, P., Pezzulla, M., Teresi, L.. Multiphysics of bio-hybrid systems: shapecontrol and electro-induced motion. *Smart Materials and Structures* 2014;**23**(4):045043. URL: http://stacks.iop.org/0964-1726/23/i=4/a=045043.

6. Aliev, R.R., Panfilov, A.V.. A simple two-variable model of cardiac excitation. *Chaos, Solitons & Fractals* 1996;**7**(3):293–301. URL: http://www.sciencedirect.com/science/article/pii/0960077995000895.
7. Nardinocchi, P., Teresi, L.. On the active response of soft living tissues. *Journal of Elasticity* 2007;**88**(1):27–39. URL: http://dx.doi.org/10.1007/s10659-007-9111-7.
8. Ogden, R.. *Nonlinear Elastic Deformation*. Dover, New York; 1984.
9. Timoshenko, S.. Analysis of bi-metal thermostats. *J Opt Soc Am* 1925;**11**(3):233–255. URL: http://www.opticsinfobase.org/abstract.cfm?URI=josa-11-3-233. doi:10.1364/JOSA.11.000233.
10. Armon, S., Efrati, E., Kupferman, R., Sharon, E.. Geometry and mechanics in the opening of chiral seed pods. *Science* 2011; **333**(6050):1726–1730. URL: http://www.sciencemag.org/content/333/6050/1726.full.pdf. doi:10.1126/science.1203874.
11. Erb, R.M., Sander, J.S., Grisch, R., Studart, A.R.. Self-shaping composites with programmable bioinspired microstructures. *Nat Commun* 2013;**4**:1712–1719. URL: http://dx.doi.org/10.1038/ncomms2666.
12. Teresi, L., Varano, V.. Modeling helicoid to spiral-ribbon transitions of twist-nematic elastomers. *Soft Matter* 2013;**9**:3081–3088. URL: http://dx.doi.org/10.1039/C3SM27491H. doi:10.1039/C3SM27491H.